JACS
JOURNAL OF THE AMERICAN CHEMICAL SOCIETY
Article
pubs.acs.org/JACS

Nanometer-Size Effect on Hydrogen Sites in Palladium Lattice

Hiroshi Akiba,[†] Maiko Kofu,[†] Hirokazu Kobayashi,[‡] Hiroshi Kitagawa,[‡] Kazutaka Ikeda,[§] Toshiya Otomo,[§] and Osamu Yamamuro*[,†]

[†]Institute for Solid State Physics, University of Tokyo, 5-1-5 Kashiwanoha, Kashiwa, Chiba, 277-8581, Japan

[‡]Department of Chemistry, Graduate School of Science, Kyoto University, Kitashirakawa Oiwake-cho, Sakyo-ku, Kyoto 606-8502, Japan

[§]Institute of Materials Structure Science, High Energy Accelerator Research Organization, 203-1 Shirakata, Tokai, Ibaraki 319-1106, Japan

Supporting Information

ABSTRACT: Nanometer-sized materials attract much attention because their physical and chemical properties are substantially different from those of bulk materials owing to their size and surface effects. In this work, neutron powder diffraction experiments on the nanoparticles of palladium hydride, which is the most popular metal hydride, have been performed at 300, 150, and 44 K to investigate the positions of the hydrogen atoms in the face-centered cubic (fcc) lattice of palladium. We used high-quality $PdD_{0.363}$ nanocrystals with a diameter of 8.0 ± 0.9 nm. The Rietveld analysis revealed that 30% of D atoms are located at the tetrahedral (T) sites and 70% at the octahedral (O) sites. In contrast, only the O sites are occupied in bulk palladium hydride and in most fcc metal hydrides. The temperature dependence of the T-site occupancy suggested that the T-sites are occupied only in a limited part, probably in the subsurface region, of the nanoparticles. This is the first study to determine the hydrogen sites in metal nanoparticles.

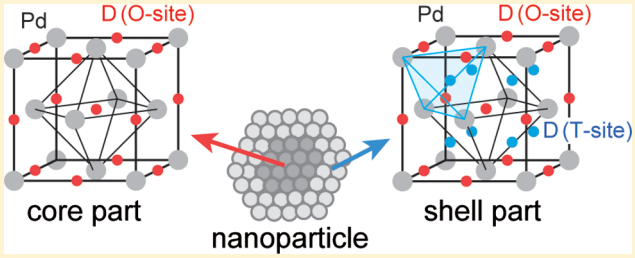

INTRODUCTION

Palladium absorbs plenty of hydrogen (PdH_x: $x > 0.6$) at an ambient condition and so has been remarked from various industrial points of view, for example, hydrogen storage, filters, sensors, catalysts, and so forth. Palladium hydride has attracted much attention also from physical interests, for example, the 50 K anomaly,[1] quantum diffusion of hydrogen,[2] superconductivity at higher hydrogen composition,[3] and so forth. Thus, palladium hydride, which may be the most well-known and classical metal hydride, is still one of the most important metal hydrides in various fields.

On the absorption process of hydrogen into palladium, a hydrogen molecule (H_2) dissociates into two hydrogen atoms (2H), and the H atoms occupy the interstitial sites of a face-centered cubic (fcc) lattice (space group: $Fm\bar{3}m$). The Pd lattice has two possible interstitial sites for H atoms, that is, octahedral (O) sites (1/2, 1/2, 1/2) and tetrahedral (T) sites (1/4, 1/4, 1/4), as shown in Figure 1. Palladium hydride has two fcc phases depending on its hydrogen composition x. At around room temperature, the α phase is stable at $x < 0.02$, while the β phase is stable at $x > 0.6$; the two phases coexist at $0.02 < x < 0.6$.[4,5] The volume of the β phase is 11% larger than that of the α phase.[6] In the β phase, it is known that the H atoms are located only at the O-sites at ambient temperature and H_2 pressure.[7] In other transition metals with the fcc lattice, H atoms also preferentially occupy the O-site which has a larger free space than the T-site.[8] In high-temperature or high-pressure conditions, however, the T-sites are partially occupied,[9−11] for example, 14% of D atoms are located at the T-sites at 582 K and 6.9 MPa in PdD_x[9] and 17% at 988 K and 6.3 GPa in FeD_x.[11]

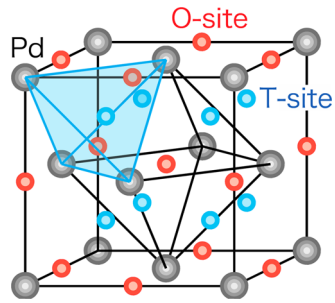

Figure 1. Structure of the β phase of palladium hydride. The gray spheres represent the fcc lattice of Pd. The red and blue spheres show the possible octahedral and tetrahedral sites for accommodated hydrogen atoms, respectively.

There have been several important experiments about the hydrogen adsorption processes on Pd surfaces.[12−14] The thermal desorption spectroscopy and nuclear reaction analysis using a $^{15}N^{2+}$ ion beam, which is H-specific and depth-resolving, revealed that H atoms are stabilized near the surface

Received: May 22, 2016
Published: July 27, 2016

DOI: 10.1021/jacs.6b04970
J. Am. Chem. Soc. 2016, 138, 10238−10243

called "subsurface". The hydrogenation reactions with the H or D atoms supplied from the subsurface were actually observed in some systems.[15,16] However, the crystallographic sites accommodating H or D atoms at the subsurface have not been clarified yet. The effect of subsurface should be prominent in nanoparticles with large surfaces.

The physical and chemical properties of nanometer-sized materials are often different from the corresponding bulk properties.[17,18] As for the nanoparticles of PdH_x, there are drastic changes in the phase diagram (H_2 pressure−composition isotherms),[19−22] lattice expansion by hydrogen absorption,[23,24] heat capacity,[25] and so forth. The phase diagram[19−22] shows that the hydrogen storage capacity decreases and that the $\alpha-\beta$ coexisting region becomes narrower with decreasing the particle size. The X-ray powder diffraction (XRPD) works[23,24] demonstrated that the difference in the lattice constant between the α and β phases also becomes smaller as the particle size decreases. Recently, we found that the 50 K anomaly in the heat capacity of bulk PdH_x is attributed to a glass transition corresponding to the freezing of the jump motions of H atoms in the Pd lattice, and this glass transition disappears in nanoparticles of PdH_x.[25] To understand the characteristic properties of Pd nanoparticles from the microscopic point of view, it is first necessary to investigate the structure including the location of hydrogen atoms. In this study, therefore, we have performed the neutron powder diffraction (NPD) measurements for nanoparticles of $PdD_{0.363}$ by using high-quality nanoparticles and a modern high-spec NPD instrument.

The cross section of X-ray scattering is roughly proportional to the square of the atomic number while that of neutron scattering is comparable for all atoms because neutrons are scattered by atomic nuclei. Hence, the neutron diffraction is superior for the observation of light atoms involved in materials consisting of heavy atoms. In the present case, the coherent cross sections σ_{coh} of Pd and D atoms are 4.39×10^{-28} m^2 and 5.59×10^{-28} m^2, respectively. The deuterated sample is used because a H atom has a relatively small σ_{coh} ($=1.76 \times 10^{-28}$ m^2) and a large incoherent scattering cross section ($\sigma_{inc} = 80.27 \times 10^{-28}$ m^2) which produces significant background.

EXPERIMENTAL SECTION

The Pd nanoparticles used in the present experiment were obtained by the solution reduction method.[25,26] A transmission electron microscope (TEM) photograph[25] revealed that the obtained nanoparticles had a well-defined shape of an edge-cut octahedron and were monodisperse. The diameter of the nanoparticles was determined to be 8.0 ± 0.9 nm by measuring those of 700 particles in the TEM images. The nanoparticles were covered with a protective polymer polyvinylpyrrolidone (PVP) to avoid adhesion between the nanoparticles. The mass of the sample including PVP was 773 mg. The mass ratio of Pd and PVP was determined by an elemental analysis to be 74.5:25.5.

The NPD measurements were performed using a time-of-flight (TOF) high intensity total diffractometer (NOVA) installed at MLF (Materials and Life Science Experimental Facility), J-PARC (Japan Proton Accelerator Research Complex). The merit of NOVA is its high intensity, which is required for a small amount of sample such as nanoparticles. Another merit is that a pressure−composition−temperature (PCT) measurement system is installed to the cryostat to make in-situ determination of the hydrogen composition of the samples.

The powder sample of the Pd nanoparticles was loaded into a vanadium cell (diameter: 7.8 mm, volume: 1.6 cc) and was evacuated at 100 °C for ca. 1 day to remove the water and air adsorbed on the nanoparticle surfaces and also a small amount of hydrogen occluded inside the nanoparticles. Then, D_2 gas was introduced into the nanoparticles at 300 K and 0.11 MPa. During the D_2 gas absorption, the pressure change in the sample cell was monitored to determine the amount of the absorbed gas. This process is shown in Figure S1. It took ca. 5 h to obtain the equilibrium state. The D composition x was calculated to be 0.363.

The diffraction data of the $PdD_{0.363}$ nanoparticles were collected for 12 h at 300, 150, and 44 K which is the lowest temperature of the cryostat. For the correction of the data, the diffraction data of PVP and empty cell were separately measured at 300 K. Figure S2 shows the contribution from each part. The contribution from $PdD_{0.363}$ is small (ca. 10%) owing to large incoherent scatterings from PVP and the vanadium cell. Thus, the present experiment is not easy from the aspect of the counting statistics. For comparison, the diffraction pattern of bulk $PdD_{0.667}$ (STREM CHEMICALS, ca. 500 mg) was also measured at 298 K. The crystal structures of bulk and nanoparticle PdD_x samples were investigated by the Rietveld analyses using the Z-Rietveld software.[27,28]

RESULTS AND DISCUSSION

Neutron Diffraction Patterns and Rietveld Analyses. Figure 2 shows the diffraction patterns of (a) bulk and (b) nanoparticles of Pd and PdD_x measured at room temperature. The diffraction peaks observed for the nanoparticles were broader than those for the bulk sample. There is a clear difference in the diffraction patterns between Pd and PdD_x both for the bulk and nanoparticle samples, indicating a large contribution from D atoms in the neutron diffraction. The peak positions of PdD_x were shifted to the lower Q side from those of Pd, reflecting the lattice expansion owing to the D_2 absorption. The diffraction data of the nanoparticles were extracted by subtracting the large incoherent scattering from the H atoms in PVP and the vanadium cell. The contribution of PVP is more than 10 times larger than the most intense diffraction peak from the Pd nanoparticles, as shown in Figure S2. This unwelcome situation negatively affects the quality of the data plotted in Figure 2b.

The result of the Rietveld analysis for bulk $PdD_{0.67}$ demonstrated that D atoms occupy only the octahedral sites of the fcc lattice as expected from previous diffraction works[7] (see Figure S3). The results for the nanoparticles of Pd and $PdD_{0.363}$ are shown in Figures 3 and 4, respectively. All of the fittings were performed on the basis of the fcc structure (space group: $Fm\bar{3}m$). The observed peak shape was described by a pseudo-Voigt profile function. Other than the structural parameters depending on the models, the following variable parameters were refined: a lattice constant, 13 background parameters, 20 peak profile parameters, and a scale factor. The details of the refinements are given in the Supporting Information. The important refined structural parameters and S values ($=R_{wp}/R_e$) are summarized in Table 1.

Structure of Pd Nanoparticle. Figure 3a shows the result for the Pd nanoparticles assuming the same model as in the bulk Pd (model 1). The fitting was not satisfactory ($S = 1.51$). In the next fitting, therefore, the hypothetical phase separation

DOI: 10.1021/jacs.6b04970
J. Am. Chem. Soc. 2016, 138, 10238−10243

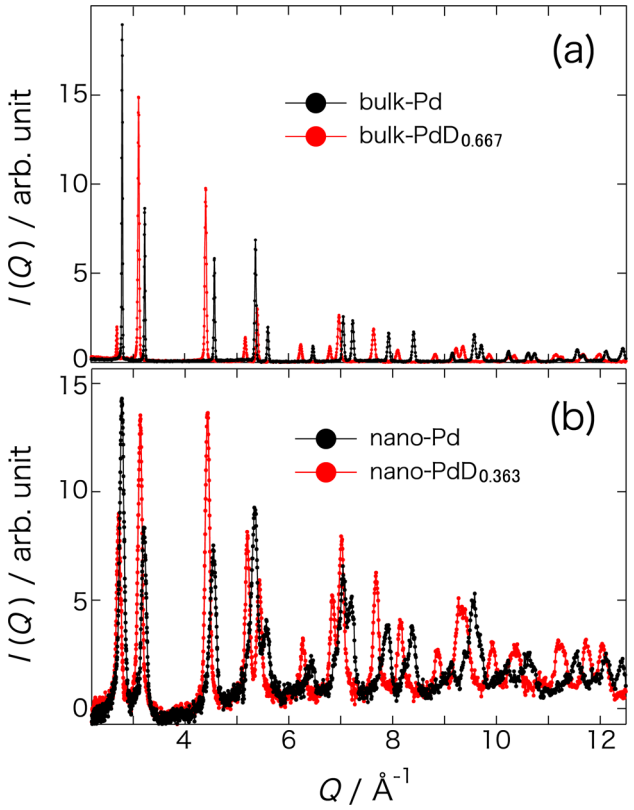

Figure 2. (a) Neutron powder diffraction patterns of bulk Pd (black) and $PdD_{0.667}$ (red) measured at 298 K under vacuum and 0.11 MPa of D_2 gas. (b) Neutron diffraction patterns of the nanoparticles of Pd (black) and $PdD_{0.363}$ (red) measured at 300 K under the same conditions as a.

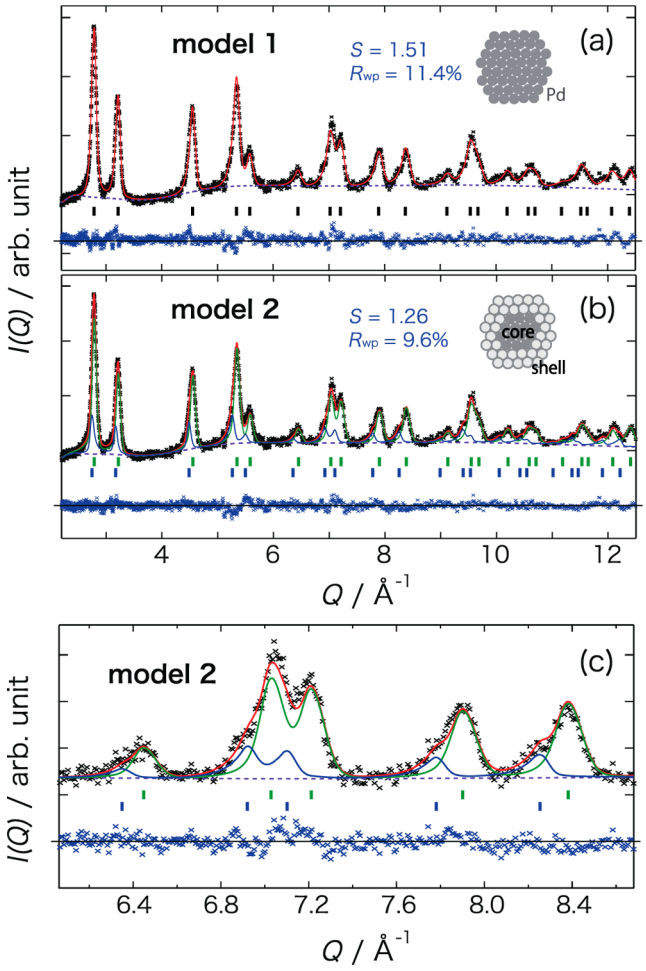

Figure 3. Observed (black crosses) and calculated (red curves) diffraction patterns of the Pd nanoparticles at 300 K. The peak positions calculated on the basis of the $Fm\bar{3}m$ space group are given by the vertical bars (tick marks), and the differences between the observed and calculated intensities are shown by the blue crosses. The Rietveld analyses were performed assuming (a) the same structure as bulk Pd and (b) the phase separation between the core and shell parts of the nanoparticles, each corresponding to the green and blue curves and tick marks, respectively. The insets show the schematic structural models. (c) The enlarged graph around $Q = 7$ Å^{-1}. See text for details.

between the core and shell region was assumed to incorporate the surface effect of the nanoparticles (model 2). The fitting was essentially improved as shown in Figure 3b ($S = 1.26$). The lattice constant of the shell part ($a_S = 3.9632$ Å) is 1.5% larger than that of the core part ($a_C = 3.9026$ Å). The Pd atomic fraction of the shell part f_S was determined to be 0.24, which corresponds to the two atomic layers near the surface assuming a spherical nanoparticle with a diameter of 8 nm. In Figure 3c, the effect of the shell part is demonstrated as the shoulders of the main peaks on the low Q side.

The particle size (diameter) L of the Pd nanoparticles was estimated to be 6.3 nm from the Scherrer equation[29,30] $L = 2\pi k/\Delta Q$ where k is a Scherrer constant (=0.9 for cubic particles) and ΔQ is a full width at half-maximum of the diffraction peak (=0.089 Å^{-1} for the core part). This value is quite consistent with the one obtained from the TEM observation (8.0 nm) taking the ambiguity due to the surface effect into consideration. As shown in the following section, the peak width was not changed by absorbing D_2 gas.

The lattice constants of the Pd nanoparticles shown earlier are essentially larger than that of bulk Pd (3.8894 Å). This is contrary to the general size dependence of the lattice constant of metals,[31−34] as pointed out in previous X-ray diffraction works.[20,35]

D Atom Positions in Pd Nanoparticles. The structural models 1−4 for the $PdD_{0.363}$ nanoparticles have been tested as shown in Figure 4a−d, respectively. In model 1, the D atoms occupy only the O-sites of the fcc lattice as in bulk PdD_x. The D atom occupancy was fixed at the value corresponding to x = 0.363 determined from the PCT measurement (see Figure S1). The fitting was not satisfactory, especially in the low-Q region. In model 2, the core and shell parts with different D compositions were assumed; D atoms occupy the O-sites in both parts. This model is referred to the experimental results mentioned in the Introduction; H atoms are preferentially located at the subsurface.[12−16] In the course of fitting, all of the D atoms moved to the shell part. The fitting with model 2 was still not satisfactory as shown by the deviation in Figure 4b. In model 3, both the O-sites and T-sites are occupied by the D atoms homogeneously. Model 3 yields a considerably better fitting than model 1 and model 2. In model 4, the T-site occupancy was introduced only in the subsurface region, that is, both the O-sites and T-sites are occupied in the shell part, while only the O-sites are occupied in the core part. To stabilize this fitting, the Pd atomic fraction of shell part f_S was fixed to a reasonable value of 0.24, which is the same as in the fitting of the D atom free Pd nanoparticles (Figure 3b); the refinement taking f_S as a flexible parameter did not improve the S value.

DOI: 10.1021/jacs.6b04970
J. Am. Chem. Soc. 2016, 138, 10238−10243

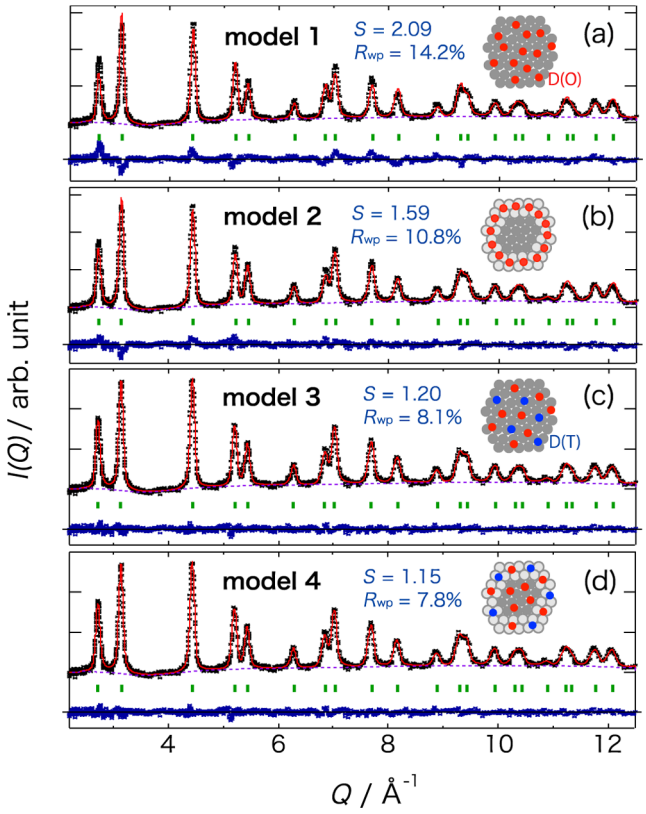

Figure 4. Observed (black crosses) and calculated (red curves) diffraction patterns of the nanoparticles of $PdD_{0.363}$ at 300 K. The peak positions calculated on the basis of $Fm\bar{3}m$ space group are given by the green tick marks, and the differences between the observed and calculated intensities are shown by the blue crosses. The Rietveld analyses for the nanoparticle $PdD_{0.363}$ were performed assuming that D atoms are located at (a) the O-sites homogeneously, (b) the O-sites only in the shell part, (c) both the O- and T-sites homogeneously, and (d) the O- and T-sites in the shell part and the O-sites in the core part. The insets show the schematic structural models. The gray circles represent the Pd atoms, and the red and blue circles show the D atoms at the O- and T-sites, respectively. See text for the details of the models.

The best-fit result was obtained with model 4. The fraction of the D atoms at the T-sites is defined as

$$n_T = \frac{f_S x_{S(T)}}{(1 - f_S)x_{C(O)} + f_S[x_{S(O)} + x_{S(T)}]} \quad (1)$$

where x_S (at the T or O site) and x_C (O site only) are the partial compositions of the shell and core parts, respectively. The determined value of n_T is 0.309 at 300 K and 0.1 MPa. Though there was no significant improvement of the S value compared with model 3, model 4 is required to explain the temperature dependence of n_T as described later. Thus, our neutron diffraction experiment has revealed that the D atoms occupy not only the O-sites but also the T-sites in Pd nanoparticles.

The temperature factors of the D atoms $B_{D(T)}$ at the T sites are too large in models 3 and 4. This suggests that the D atoms are located at the general positions slightly deviated from the T sites (1/4, 1/4, 1/4) and are disordered among them. The deviated positions are probably stabilized by the surface or distortion effects of the nanoparticles. As another manner of the distribution of D atoms at the T-sites, a Gaussian distribution model may be considered. This model could roughly reproduce the experimental pattern but cannot represent the diffraction peak profile with a definite shoulder as shown in Figure 3c. Further discussion on the validity of the core−shell model is performed in the next section.

Temperature Dependence of D Atom Positions. To investigate the temperature dependence of the T-site occupancy, we performed the NPD experiment at 44 and 150 K. The clear temperature dependence was observed as shown in Figure S4. The Rietveld analyses for the low-temperature data were performed on the basis of model 4 (see Figure S5). Figure 5 shows the T-site fraction n_T obtained by the Rietveld analysis. The fraction n_T decreases with decreasing temperature, indicating that the O-site is thermodynamically more stable than the T-site. The T-site fraction seems to asymptotically approach a constant value of about 30%. In the case of model 3, the number of the T-sites is twice as many as that of the O-sites, and so n_T will become 2/3 when both sites are equally occupied at the high-temperature limit. Thus, model 3 cannot reproduce the observed temperature dependence of n_T. The

Table 1. Structural Parameters Determined by Rietveld Analyses[a]

model	sample	T/K	f_S	$x_{(O)}$[b]	$x_{(T)}$[b]	a[b]/Å	B_{Pd}/Å^2	$B_{D(O)}$/Å^2	$B_{D(T)}$/Å^2	S
1	bulk-Pd	298				3.88936(4)	0.61(1)			1.71
1	nano-Pd	300				3.917(1)	0.326(6)			1.51
2	nano-Pd	300	0.240(4)			3.9026(2)	0.323(6)			1.26
						3.9632(6)				
1	bulk-$PdD_{0.667}$	298		0.667[c]		4.03684(1)	0.675(4)	3.95(1)		1.83
1	nano-$PdD_{0.363}$	300		0.363[c]		4.0107(1)	0.265(5)	5.59(5)		2.09
2	nano-$PdD_{0.363}$	300	0.363[c]	0[c]		4.0081(3)	0.091(5)	2.68(5)		1.59
				1[c]		4.0138(2)				
3	nano-$PdD_{0.363}$	300		0.250(2)	0.113(2)	4.0109(1)	0.319(8)	1.93(6)	15.4(7)	1.20
4	nano-$PdD_{0.363}$	300	0.24[c]	0.251(2)	0	4.0027(2)	0.280(5)	1.99(6)	14.1(5)	1.15
				0.251(2)	0.468(7)	4.0177(4)				
4	nano-$PdD_{0.363}$	150	0.24[c]	0.256(2)	0	4.0014(2)	0.122(5)	1.27(4)	14.9(7)	1.20
				0.256(2)	0.444(7)	4.0175(4)				
4	nano-$PdD_{0.363}$	44	0.24[c]	0.274(1)	0	3.9959(1)	0.038(4)	1.40(4)	10.7(4)	1.34
				0.274(1)	0.373(6)	4.0159(3)				

[a]The following atomic coordinates are fixed throughout the refinement: Pd(0,0,0), $D_{O\text{-site}}$(1/2,1/2,1/2), $D_{T\text{-site}}$(1/4,1/4,1/4). [b]For the columns with two lines, the upper and lower lines correspond to the values for the core and shell parts, respectively. [c]Fixed. See text for the details.

DOI: 10.1021/jacs.6b04970
J. Am. Chem. Soc. 2016, 138, 10238−10243

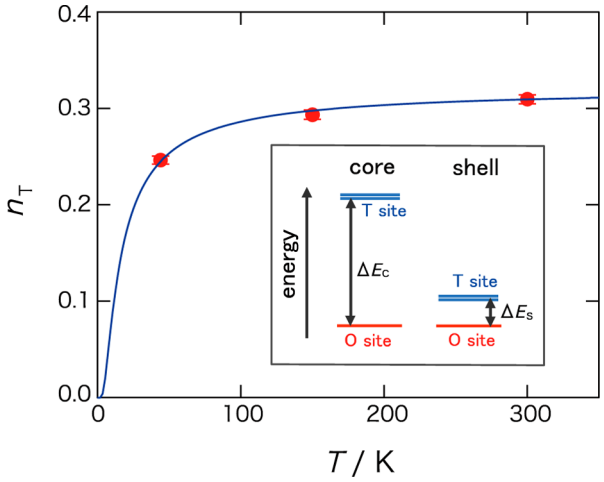

Figure 5. Temperature dependence of the fraction of the D atoms at the T-sites determined by the Rietveld analysis. The inset shows the schematic energy diagram based on model 4. The blue curve shows the result of the fitting to eq 2. See text for details.

Gaussian distribution model also does not represent the saturation value of 30%.

The inset of Figure 5 shows the schematic energy diagram of the O-site and T-site on the basis of the core−shell model (model 4). Here, we assumed that the T-sites are stabilized only in the shell part, and so the energy difference ΔE_S between the O and T sites in the shell part is significantly smaller than that in the core part ΔE_C. The levels of the O sites for the core and shell parts are set to be equivalent for descriptive purposes, but they may be different from each other. The mechanism for stabilizing the T site in the shell part is not clear but could be related to the fact that the lattice constant of the shell part is larger than that of the core part. For most d-band metals, it is known that the volume expansion caused by a hydrogen atom at the T-site is larger than that at the O-site.[8] Such effect of the lattice expansion is also found in the density functional theory study on PdH.[36] The population of the T-sites on the basis of this energy diagram is described by the Boltzmann distribution:

$$n_T = \frac{2f_S \exp(-\Delta E_S/k_B T)}{1 + 2f_S \exp(-\Delta E_S/k_B T)} \quad (2)$$

Here, the population in the core part is omitted because ΔE_C is much larger than $k_B T$. The observed n_T was fitted to eq 2 using ΔE_S as a fitting parameter; the atomic fraction of the shell part f_S was fixed to be 0.24. The result of the fit is good as shown by the blue solid curve in Figure 5. The f_S value other than the present one (=0.24) cannot reproduce the observed temperature dependence of n_T. This fact supports the validity of the core−shell model. The determined $\Delta E_S/k_B$ was estimated to be 16.6 K. This value seems to be too small taking account of the fact that D atoms are accommodated only in the O sites in the core region of the nanoparticles; the surface effect is too drastic. It is possible that the n_T value at 44 K, which mainly causes very small ΔE_S, is not of equilibrium, but the hopping motion of D atoms is frozen at some temperature above 44 K. An NPD experiment below 44 K is required.

CONCLUSION

The NPD experiments on the nanoparticle $PdD_{0.363}$ have been performed at 300, 150, and 44 K. The Rietveld analyses revealed that ca. 30% of D atoms are located at the T-sites and 70% at the O-sites. The temperature dependence of the fraction suggested that the T-site occupation occurs only in the subsurface (about two layers near the surface) of the nanoparticles. We guess that the T-sites are stabilized by the surface or distortion effects of the nanoparticles. The locations of the hydrogen sites in metal nanoparticles were determined for the first time by the present study.

The present situation for the D atom positions will cause drastic changes on the diffusional and vibrational motions of the hydrogen atoms in Pd nanoparticles. The quasielastic and inelastic neutron scattering studies using the same nanoparticle sample are now in progress.

ASSOCIATED CONTENT

Supporting Information

The Supporting Information is available free of charge on the ACS Publications website at DOI: 10.1021/jacs.6b04970.

D_2 gas absorption process into Pd nanoparticles, additional neutron diffraction data for the bulk samples and nanoparticle samples at low temperature, and details for all of the Rietveld refinements in this work (PDF)

AUTHOR INFORMATION

Corresponding Author

*yamamuro@issp.u-tokyo.ac.jp

Notes

The authors declare no competing financial interest.

ACKNOWLEDGMENTS

The experiment in the MLF at J-PARC was performed with the approval of J-PARC (Proposal No. 2012B0246, 2013A0086). This work is financially supported by CREST, Japan Science and Technology Agency.

REFERENCES

(1) Nace, D. M.; Aston, J. G. *J. Am. Chem. Soc.* **1957**, *79*, 3627−3633.
(2) Svare, I. *Physica B+C* **1986**, *141*, 271−276.
(3) Skoskiewicz, T. *Phys. Stat. Sol. (a)* **1972**, *11*, K123−K126.
(4) Frieske, H.; Wicke, E. *Ber. Bunsenges. Phys. Chem.* **1973**, *77*, 48−52.
(5) Lässer, R.; Klatt, K. − H. *Phys. Rev. B: Condens. Matter Mater. Phys.* **1983**, *28*, 748−758.
(6) Aben, P.; Burgers, W. G. *Trans. Faraday Soc.* **1962**, *58*, 1989−1992.
(7) Worsham, J. E.; Wilkinson, M. K.; Shull, C. G. *J. Phys. Chem. Solids* **1957**, *3*, 303−310.
(8) Fukai, Y. *The Metal-Hydrogen System*; Springer: Berlin, 2005.
(9) Pitt, M. P.; Gray, E. M. *Europhys. Lett.* **2003**, *64*, 344−350.
(10) McLennan, K. G.; Gray, E. M.; Dobson, J. F. *Phys. Rev. B: Condens. Matter Mater. Phys.* **2008**, *78*, 014104.
(11) Machida, A.; Saitoh, H.; Sugimoto, H.; Hattori, T.; Sano-Furukawa, A.; Endo, N.; Katayama, Y.; Iizuka, R.; Sato, T.; Matsuo, M.; Orimo, S.; Aoki, K. *Nat. Commun.* **2014**, *5*, 5063.
(12) Behm, R. J.; Penka, V.; Cattania, M.-G.; Christmann, K.; Ertl, G. *J. Chem. Phys.* **1983**, *78*, 7486−7490.
(13) Rieder, K. H.; Baumberger, M.; Stocker, W. *Phys. Rev. Lett.* **1983**, *51*, 1799−1802.
(14) Wilde, M.; Fukutani, K. *Phys. Rev. B: Condens. Matter Mater. Phys.* **2008**, *78*, 115411.
(15) Ogura, S.; Okada, M.; Fukutani, K. *J. Phys. Chem. C* **2015**, *119*, 23973−23977.

DOI: 10.1021/jacs.6b04970
J. Am. Chem. Soc. 2016, 138, 10238−10243

(16) Teschner, D.; Borsodi, J.; Wootsch, A.; Révay, Z.; Hävecker, M.; Knop-Gericke, A.; Jackson, S. D.; Schlögl, D. *Science* **2008**, *320*, 86−89.
(17) Schmid, G. *Clusters and Colloids*; VCH: Weinheim, Germany, 1994.
(18) Sugano, S.; Koizumi, H. *Microcluster Physics*; Springer: Berlin, 1998.
(19) Sachs, C.; Pundt, A.; Kirchheim, R.; Winter, M.; Reetz, M. T.; Fritsch, D. *Phys. Rev. B: Condens. Matter Mater. Phys.* **2001**, *64*, 075408.
(20) Yamauchi, M.; Ikeda, R.; Kitagawa, H.; Takata, M. *J. Phys. Chem. C* **2008**, *112*, 3294−3299.
(21) Bardhan, R.; Hedges, L. O.; Pint, C. L.; Javey, A.; Whitelam, S.; Urban, J. J. *Nat. Mater.* **2013**, *12*, 905−912.
(22) Griessen, R.; Strohfeldt, N.; Giessen, H. *Nat. Mater.* **2016**, *15*, 311−317.
(23) Ingham, B.; Toney, M. F.; Hendy, S. C.; Cox, T.; Fong, D. D.; Eastman, J. A.; Fuoss, P. H.; Stevens, K. J.; Lassesson, A.; Brown, S. A.; Ryan, M. P. *Phys. Rev. B: Condens. Matter Mater. Phys.* **2008**, *78*, 245408.
(24) Suleiman, M.; Jisrawi, N. M.; Dankert, O.; Reetz, M. T.; Bähtz, C.; Kirchheim, R.; Pundt, A. *J. Alloys Compd.* **2003**, *356*−*357*, 644−648.
(25) Akiba, H.; Kobayashi, H.; Kitagawa, H.; Kofu, M.; Yamamuro, O. *Phys. Rev. B: Condens. Matter Mater. Phys.* **2015**, *92*, 064202.
(26) Lim, B.; Jiang, M.; Camargo, P. H. C.; Cho, E. C.; Tao, J.; Lu, X.; Zhu, Y.; Xia, Y. *Science* **2009**, *324*, 1302−1305.
(27) Oishi, R.; Yonemura, M.; Nishimaki, Y.; Torii, S.; Hoshikawa, A.; Ishigaki, T.; Morishima, T.; Mori, K.; Kamiyama, T. *Nucl. Instrum. Methods Phys. Res., Sect. A* **2009**, *600*, 94−96.
(28) Oishi-Tomiyasu, R.; Yonemura, M.; Morishima, T.; Hoshikawa, A.; Torii, S.; Ishigaki, T.; Kamiyama, T. *J. Appl. Crystallogr.* **2012**, *45*, 299−308.
(29) Scherrer, P. *Nachr. Ges. Wiss. Göttingen, Math.-Phys. Kl.* **1918**, 98−100.
(30) Warren, B. E. *X-ray Diffraction*; Addison-Wesley: New York, 1969.
(31) Zhang, P.; Sham, T. K. *Phys. Rev. Lett.* **2003**, *90*, 245502.
(32) Apai, G.; Hamilton, J. F.; Stohr, J.; Thompson, A. *Phys. Rev. Lett.* **1979**, *43*, 165.
(33) Montano, P. A.; Schulze, W.; Tesche, B.; Shenoy, G. K.; Morrison, T. I. *Phys. Rev. B: Condens. Matter Mater. Phys.* **1984**, *30*, 672.
(34) Solliard, C.; Flueli, M. *Surf. Sci.* **1985**, *156*, 487.
(35) Teranishi, T.; Miyake, M. *Chem. Mater.* **1998**, *10*, 594−600.
(36) Grönbeck, H.; Zhdanov, V. P. *Phys. Rev. B: Condens. Matter Mater. Phys.* **2011**, *84*, 052301.

DOI: 10.1021/jacs.6b04970
J. Am. Chem. Soc. 2016, 138, 10238−10243